

**Using a vapor-fed anode and saline catholyte to manage ion transport in a proton exchange membrane electrolyzer**

Journal:	<i>Energy & Environmental Science</i>
Manuscript ID	EE-ART-07-2021-002265.R1
Article Type:	Paper
Date Submitted by the Author:	21-Sep-2021
Complete List of Authors:	Rossi, Ruggero; Penn State University Park Hall, Derek; Pennsylvania State University, Department of Energy and Mineral Engineering; Pennsylvania State University, EMS Energy Institute Shi, Le; Penn State, Civil & Environmental Engineering Cross, Nicholas; Pennsylvania State University, Department of Energy and Mineral Engineering Gorski, Christopher; Penn State, Civil and Environmental Engineering Hickner, Michael; The Pennsylvania State University Department of Materials Science and Engineering, Logan, Bruce; Penn State, Civil & Environmental Engineering

1 Date: September 15, 2021

2 Submitted to: *Energy and Environmental Science*

3

4 **Using a vapor-fed anode and saline catholyte to manage ion transport in a proton exchange**
5 **membrane electrolyzer**

6

7 Ruggero Rossi¹, Derek M. Hall², Le Shi¹, Nicholas Cross¹, Christopher A. Gorski¹, Michael A. Hickner³,
8 Bruce E. Logan^{1*}

9

10 ¹Department of Civil and Environmental Engineering, The Pennsylvania State University, University Park, PA, USA.

11 ²Department of Energy and Mineral Engineering, The Pennsylvania State University, University Park, PA, USA.

12 ³Department of Materials Science and Engineering, The Pennsylvania State University, University Park, PA, USA.

13

14 *Corresponding author: blogan@psu.edu.

15

16

17 **Abstract**

18 Saline water represents an inexhaustible source of water for hydrogen production from electrolysis.
19 However, direct saltwater splitting faces challenges due to chlorine evolution at the anode and the
20 development of Nernst overpotential due to sodium ion transport competition with protons across the
21 membrane. A new approach to minimize chlorine evolution and improve performance is proposed here
22 by using a humidified gas stream (no liquid electrolyte) for the anode and a liquid saltwater catholyte.
23 Charge repulsion of chloride ions by the proton exchange membrane (PEM) resulted in low chlorine
24 generation, with anodic faradaic efficiencies for oxygen evolution of $100 \pm 1\%$ with a synthetic brackish
25 water (50 mM NaCl, 3 g L⁻¹) and $96 \pm 2\%$ with synthetic seawater (0.5 M NaCl, 30 g L⁻¹). The enhanced
26 proton transport by the electric field enabled more efficient pH control across the cell, minimizing sodium
27 ion transport in the absence of a liquid anolyte. The vapor-fed anode configuration showed similar
28 performance to a conventional PEM electrolyzer up to 1 A cm⁻² when both anode and cathode were fed
29 with deionized water. Much lower overpotentials could be achieved using the vapor-fed anode compared
30 to a liquid-anolyte due to the reduced sodium ion transport through the membranes, as shown by adding
31 NaClO₄ to the electrolytes. This vapor-fed anode configuration allows for direct use of saltwater in
32 conventional electrolyzers without additional water purification at high faradaic efficiencies.

33

34 **Broader context**

35 Hydrogen gas produced in water electrolyzers requires the use of ultrapure water to avoid contamination
36 of the membrane and the production of hazardous chemicals such as chlorine at the anode. It is shown

37 here that impure, saline water feeds can be used in in a water electrolyzer by feeding the saline liquid into
38 only the cathode chamber and using a vapor feed for the anode, taking advantage of the direction of the
39 electric field and the membrane charge to limit the development of concentration gradients and the
40 generation of chlorine gas. The electrolyzer fed with vapor at the anode and saline water at the cathode
41 showed high faradaic efficiency toward the oxygen evolution reaction, as the Cl^- ions in the catholyte were
42 rejected by the membrane charge, while the electrons transported from anode to cathode limited the
43 diffusion of sodium in the membrane and the development of concentration gradients across the cell.
44 These results show that that by using appropriate configuration, impure water feeds can be used in
45 water electrolyzers with little to no change in the cell performance.

46

47 **Introduction**

48 Hydrogen gas is a critical component of our energy infrastructure but is typically produced through
49 steam reforming of methane.¹ To reduce fossil fuel consumption and carbon dioxide emissions, hydrogen
50 gas produced by water electrolysis and renewable electricity will become increasingly important as a
51 chemical source for fertilizer production and as an energy carrier for transportation and large-scale grid
52 storage.^{2,3} While progress in solar energy technologies has decreased the cost of renewable electricity,
53 providing both a clean and inexpensive source of electricity, the scarcity of suitable water for electrolysis
54 in many locations remains a challenge.^{2,4–7} Typical water electrolyzers use highly purified feeds, requiring
55 ancillary equipment that increases the investments and operational energy costs and overall process
56 complexity. One strategy to avoid these additional expenditures is to develop electrolyzers that are
57 capable of directly using impure water feeds. Around 97% of surface water is saltwater,^{8–10} but it has not
58 been directly used for electrolysis due to the production of chlorine gas and reactive species, rather than
59 only oxygen at the anode.^{2,7,11} A recent analysis suggested that the overall cost for complete deionization
60 of water is a small percentage of overall costs,¹² but that viewpoint neglected the importance of
61 investment relative to capital costs as well as the impact of intermittent operations due to maintenance
62 of a specialized water treatment operation, which can result in frequent interruptions of hydrogen
63 generation in the electrolysis plant. Thus, it is worthwhile to continue to investigate water electrolysis
64 systems that can use salty water.

65 In existing PEM water electrolyzers operating under acidic conditions, any appreciable concentration
66 of chloride ions in solution, with most common catalysts, will result high chlorine evolution rates at the
67 anode due to the chlorine evolution reaction (CER) compared to the oxygen evolution reaction (OER).^{2,13,14}
68 The CER under acidic pH is typically favored over the OER. While the OER requires a lower thermodynamic

69 potential (1.23 V vs. SHE – 0.059 pH) than the CER (1.36 V) at any pH, the kinetic challenges associated
 70 with a 4 e⁻ transfer OER increases the overpotential for the oxygen evolution well above the potential
 71 required to drive chlorine evolution at low pH.¹³ The CER is a 2 e⁻ transfer reaction, characterized by
 72 exchange current density between four to seven orders of magnitude larger than that of the OER.¹³
 73 Unfortunately, Ir-based catalysts typically used in PEM electrolyzers due to their high activity toward the
 74 OER, are also extremely active for chlorine evolution, resulting in Faradaic efficiencies exceeding 86% for
 75 CER in solutions with only 30 mM NaCl.¹⁴ The chlorine generated at the anode, due to its corrosive and
 76 volatile nature can drastically reduce the lifetime of the system.^{6,10}

77 A second challenge associated with the use of impaired water for electrolysis is the competition
 78 between the cations and protons for the transport of charge across the PEM.^{11,15–18} The electrical charge
 79 due to the electron flux is typically balanced in PEM electrolyzers by the migration of the protons
 80 generated by the OER from the anode to the cathode when pure water is used as a feed. However, when
 81 impurities such as sodium ions are present in the electrolytes, electrolyzer performance is drastically
 82 reduced.^{15,16,19} Cations in the anode chamber such as Na⁺ compete with protons for transport through the
 83 PEM. For each sodium ion migrating across the PEM instead of a proton, an H⁺ generated by the OER
 84 remains in the anode proximity, lowering the local pH.²⁰ If protons are not effectively supplied to the
 85 cathode chamber, the catholyte pH increases due to the generation of hydroxide ions by the HER that are
 86 not neutralized by protons based on the following equations:



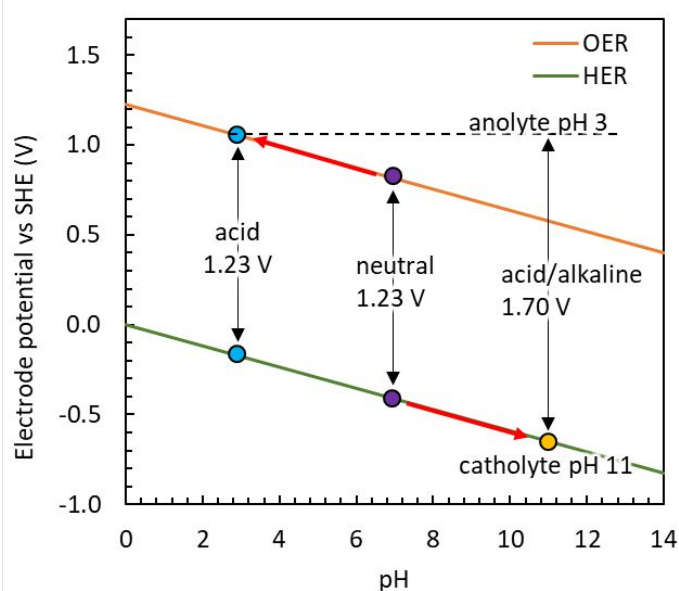
89 Thus, large pH differences can develop at the two sides of the PEM, increasing the thermodynamic
 90 potential for water splitting. This pH gradient can be described by the Nernst equation, and result in the
 91 development of Nernst overpotentials:

$$92 \quad E_{\text{OER}} = E_{0-\text{OER}} - \frac{2.303 RT}{F} \log \frac{[\text{O}_2]^{\frac{1}{4}} [\text{H}^+]}{[\text{H}_2\text{O}]^{\frac{1}{2}}} = E_{0-\text{OER}} - \frac{2.303 RT}{F} \left[\left(\log \frac{[\text{O}_2]^{\frac{1}{4}}}{[\text{H}_2\text{O}]^{\frac{1}{2}}} \right) - \text{pH} \right] \quad (3)$$

$$93 \quad E_{\text{HER}} = E_{0-\text{HER}} - \frac{2.303 RT}{F} \log \frac{[\text{H}_2]^{\frac{1}{2}} [\text{OH}^-]}{[\text{H}_2\text{O}]} = E_{0-\text{HER}} - \frac{2.303 RT}{F} \left[\left(\log \frac{[\text{H}_2]^{\frac{1}{2}}}{[\text{H}_2\text{O}]} \right) - 14 + \text{pH} \right] \quad (4)$$

94 A more acidic pH at the anode will shift the OER potential towards more positive potentials, while a more
 95 basic pH at the cathode will decrease the potential of the HER at the cathode. Under equal pH conditions
 96 in both chambers the thermodynamic potential difference between OER and HER is 1.23 V (Figure 1).^{15,16}

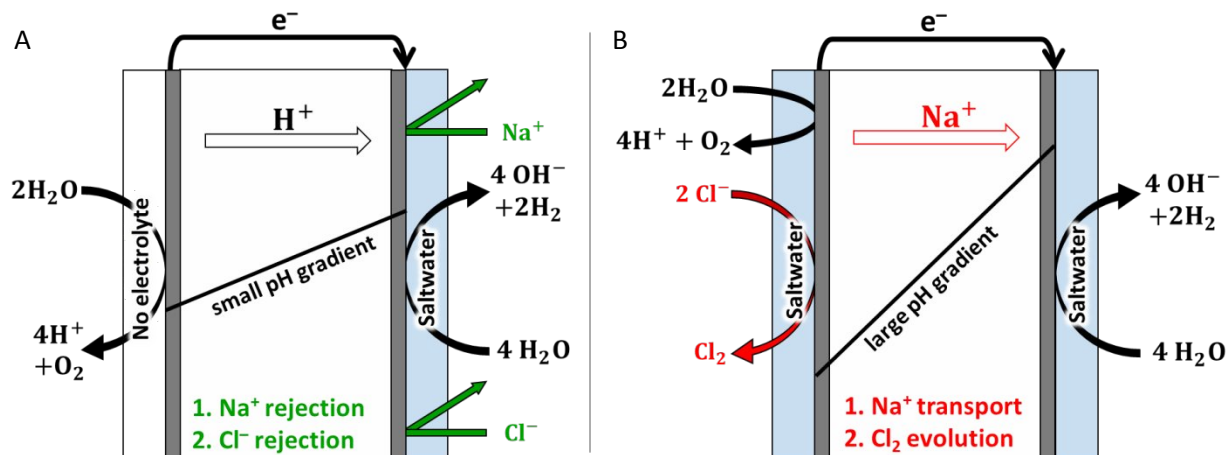
97 However, if a pH gradient develops, for example an anolyte pH of 3 and a catholyte pH of 11, then the
 98 Nernst overpotential increases the thermodynamic cell voltage to 1.70 V.



99
 100 **Figure 1.** Impact of anode and cathode pH on the thermodynamic potential for water splitting. The
 101 transport of sodium ions instead of protons can lead to anode acidification and cathode basification. Each
 102 unit of pH difference between anode and cathode increases the overpotential for water splitting by
 103 0.059 V based on the Nernst equation at standard conditions. A decrease in the anode pH from 7 to 3
 104 and an increase in the cathode pH from 7 to 11 raises the thermodynamic potential for water splitting
 105 from 1.23 V to 1.70 V.

106
 107 In this study, we developed a new and effective water electrolyzer configuration that can accept a
 108 saline water as the catholyte feed by using a vapor-fed anode chamber (Figure 2). The vapor-fed anode
 109 configuration leverages the charge of the PEM and the direction of the electric field to limit the intrusion
 110 of competing ions into the anode. The negative charges of the sulfonated moieties of the PEM limit the
 111 diffusion of Cl^- to the anode by charge repulsion, while the electric field due to the electron transport
 112 diminishes the diffusion of sodium ions to the anode as it needs to be balanced by positive ions
 113 transported from anode (vapor) to cathode (saltwater), limiting the development of large pH gradients
 114 across the PEM.²¹ The use of a vapor feeds have previously been investigated in PEM electrolyzers,^{22,23} but
 115 only by using a configuration different from that examined here. In previous studies water vapor was used
 116 as a feed for both the anode and the cathode chambers, but operation under these conditions resulted in
 117 an insufficient amount of H_2O reaching the anode, severely limiting the maximum current density of the
 118 system to only 0.04 A cm^{-2} ,^{22,23} compared to current densities two orders of magnitude larger for
 119 conventional water electrolyzers. In our configuration, the water needed for the OER at the anode is

120 provided by the vapor-feed and by water diffusing from the saline water catholyte through the
 121 membrane. The undesirable transport of chloride ions from the catholyte to the anolyte is prevented by
 122 charge repulsion of the PEM, while sodium ion transport is minimized by charge transfer of protons from
 123 the anode through the PEM, enabling high current densities.



124
 125 **Figure 2.** Comparison between a (A) water electrolyzer using a vapor feed at the anode and saltwater at
 126 the cathode and (B) water electrolyzer using saltwater at the anode and the cathode. In the vapor-fed
 127 anode configuration, only vapor is fed to the anode chamber and the PEM limits the transport of Cl⁻ from
 128 cathode to anode while the electric field restricts the transport of Na⁺, avoiding the development of large
 129 pH differences across the cell. The combined effect of Cl⁻ and Na⁺ repulsion by membrane charge and
 130 electric field direction can be obtained only in a PEM electrolyzer (Figure S1).

131

132 Materials and methods

133 Construction and operation of the water electrolyzer.

134 The cell was a 5 cm² active area electrolyzer with platinized anode Ti plate and cathode graphite plate
 135 with serpentine flow fields (Scribner Associates Inc). The catalyst inks were prepared following a method
 136 previously described using a 20% ionomer/catalyst ratio for the cathode and a 25% ionomer/catalyst ratio
 137 for the anode.²⁴ Iridium black (Alfa Aesar) was used as received as catalyst for the OER on the anode and
 138 painted on a Ti felt (thickness: 250 ± 50 μm, Fuel Cell Store) with loadings of 5 mg cm⁻². Pt on Vulcan XC72
 139 carbon (20 wt% Pt/C, BASF) was sprayed with loadings of 2.5 mg cm⁻² on carbon cloth (1071 HCB, 356 μm,
 140 Fuel Cell Store) for the HER. The membrane electrode assembly (MEA) was fabricated by hot-pressing the
 141 electrode onto Nafion® 117/212 membranes for 2 min at 130 °C at a pressure of 3000 psi. The cell was
 142 sealed at 11.5 Nm with two 254 μm thick PTFE gaskets (Scribner Associates Inc). Cell and reactant inlet
 143 temperatures were set at 80 °C.

144 Deionized (DI) water or a solution of sodium perchlorate 10 mM was used as the electrolyte for the
 145 liquid-anolyte electrolyzer to avoid chlorine evolution in some experiments. DI water, sodium perchlorate

146 10 mM, or sodium chloride (50 mM or 0.5 M) were used as catholytes in the vapor-fed anode electrolyzer
147 and pumped at 25 mL min⁻¹ except otherwise noted. The gas feed to the anode in the vapor-fed anode
148 configuration was saturated with water vapor by bubbling it at a flow rate of 25 mL min⁻¹ through a
149 reservoir that had been filled with DI and maintained at 80°C. The humidified gas stream was directly
150 pumped in the anode chamber of the vapor-fed anode electrolyzer. Ambient pressure was used for all
151 tests. The pH (Mettler Toledo) and the chlorine content (LaMotte Benchtop chlorine meter - diethyl-p-
152 phenylene diamine (DPD) colorimetric test) of the electrolytes were measured after tests and analyzed
153 immediately. The Faradaic efficiency (FE) was calculated by (1) water displacement and (2) analysis with
154 gas chromatography (GC, SRI Instrument, Torrance, CA, USA) injecting 250 µL of gas collected with gas
155 bags with an airtight syringe (Hamilton, Reno, NV, USA).

156

157 *Electrochemical characterization.*

158 The electrochemical tests were performed with a Gamry 3000 potentiostat. The polarization curves
159 were recorded with linear sweep voltammetries (LSVs) at a scan rate of 10 mV s⁻¹ until at least three
160 reproducible cycles were obtained. AC impedance measurements were recorded after the LSVs in a range
161 of 50 kHz–10 MHz at different applied potentials. A chronoamperometry (CA) was performed following
162 the impedance measurements at 0.5 A cm⁻² to investigate the impact of a constant current on the cell
163 performance. In these measurements, only current densities of up to 0.6 A cm⁻² were achieved due to
164 limitations in the potentiostat used. In a different set of experiments, a power supply (GWInstek GPR-
165 1820 HD) was used to obtain CAs at 1 A cm⁻² in the liquid-anolyte and vapor-anode configurations. Sodium
166 perchlorate 10 mM, Sodium chloride 50 mM and 0.5 M was added in the catholyte at different time during
167 the CA. The cell voltage was recorded with a MPG2 Bio-logic potentiostat.

168

169 **Results and Discussion**

170 *Vapor-fed anode versus liquid-anolyte electrolyzer performance.*

171 The vapor-fed anode configuration produced similar overpotentials relative to those measured using
172 deionized water as liquid anolyte, while it substantially improved performance in the presence of sodium
173 ions based on measured overpotentials. Using DI water at a set current of 1 A cm⁻², the cell voltage of the
174 vapor-fed anode configuration averaged 1.74 ± 0.01 V (Figure 3A), similar to that of a cell with liquid
175 electrolytes feed in the anode and cathode chambers of 1.77 ± 0.01 V (Figure 3B). The extra energy needed
176 for heating the water reservoir used to produce the water vapor fed to the anode is negligible compared
177 to the energy consumed to operate the electrolyzer. Considering a vapor feed of 25 mL min⁻¹, or 0.92 g

178 h^{-1} , the energy needed to heat the water will be 0.064 Wh, which corresponds to only 0.7% of the 8.7 Wh
179 needed to sustain a voltage of 1.74 V at a current of 5 A (1 A cm^{-2}) for one hour. To examine the impact
180 of sodium ions on the cell overpotential, in the absence of current production from chloride ion oxidation,
181 10 mM NaClO_4 was added to the liquid electrolytes. The presence of sodium ions increased the cell voltage
182 of the vapor anode electrolyzer by 9% (by 0.16 V to $1.90 \pm 0.01 \text{ V}$), compared to a much larger increase of
183 40% (0.67 V) for the liquid-anolyte electrolyzer ($2.44 \pm 0.00 \text{ V}$). The use of a vapor-fed anode has been
184 proposed in previous studies,^{22,23} however, it was coupled with a vapor-fed or a dry (N_2 gas) fed cathode,
185 which failed to provide sufficient water for the OER and the HER. As a result, the limiting current densities
186 were around two orders of magnitude ($\sim 0.04 \text{ A cm}^{-2}$) lower than that those obtained here by coupling
187 the vapor-fed anode with a saltwater feed catholyte.

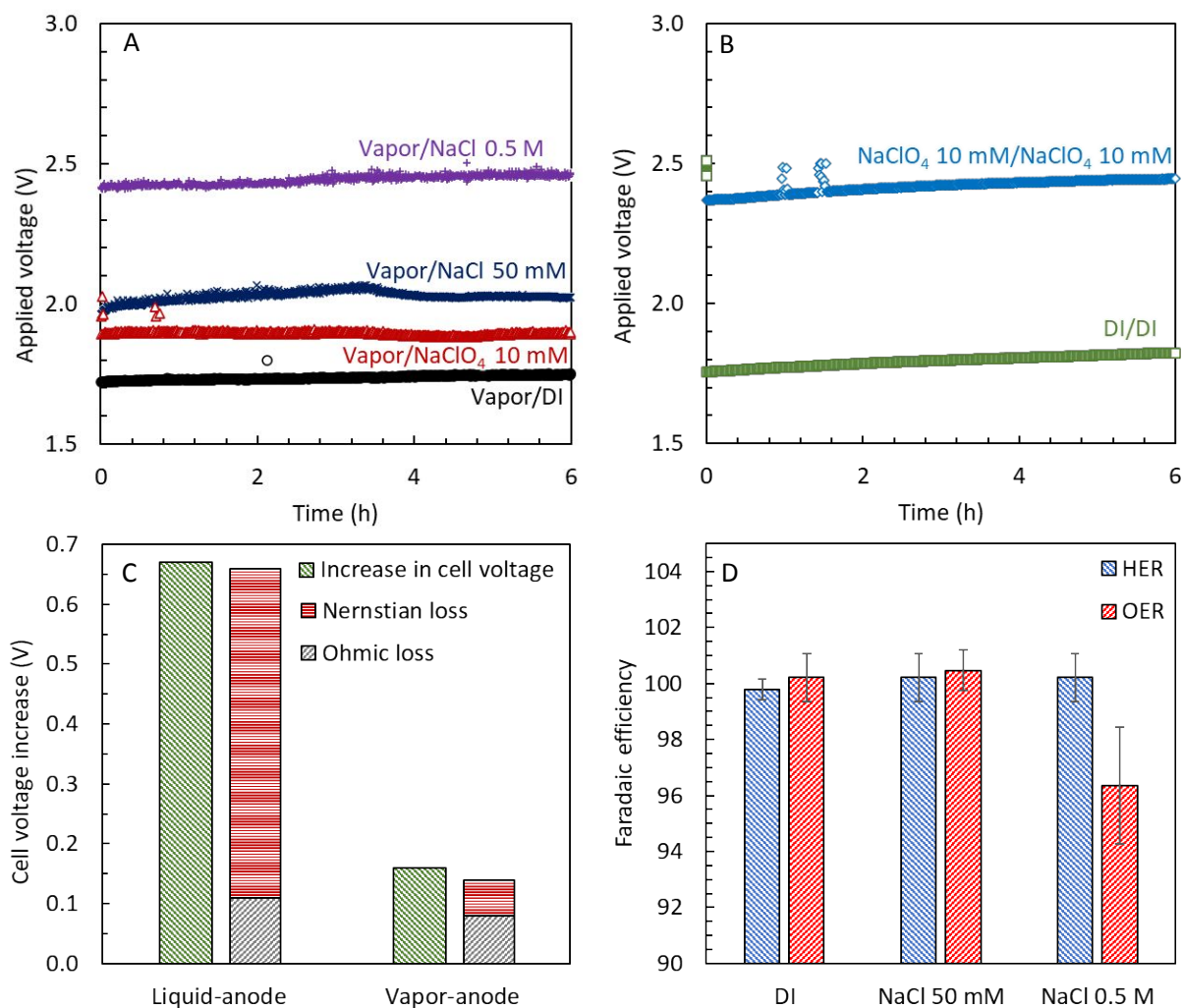


Figure 3. Chronoamperometries at 1 A cm^{-2} of the (A) vapor-fed anode and (B) liquid-anode electrolyzer using Nafion 212 with different concentrations of NaClO_4 and NaCl in the electrolyte. (C) Impact of the presence of sodium ions in solution in terms of overpotential due to pH gradient, calculated from the Nernst equation, and ohmic losses, calculated from the Ohm's law. (D) Faradaic efficiency of the vapor-fed anode electrolyzer with different NaCl concentration in the catholyte.

188

189 The largest impact of the sodium ion on performance was the increased Nernst overpotential due to
 190 pH gradient across the cell. With current generation, the electric field enhanced the migration of positive
 191 ions through the PEM to balance charge. However, the concentration of sodium ions in solution (10 mM
 192 using NaClO_4) is larger than that of protons (0.001 mM at pH 6), and their transport across the membrane
 193 is therefore favored. When a sodium ion, rather than a proton, migrates from anode to cathode to balance
 194 charge, the anolyte pH decreases (eq. 1) and the catholyte pH increases due to the release of hydroxide
 195 ions (eq. 2) that are not neutralized by protons.^{15,16,25} Thus, a large pH gradient develops across the PEM,
 196 resulting in Nernst overpotentials due to the pH differences in the cell (Figure 1). In the liquid-anolyte

197 configuration, using NaClO_4 (10 mM) to study the impact of Na^+ ion separately from impacts of the CER,
198 the solution pH shifted from a pH of 6.0 in both electrolytes to 2.5 in the anolyte and to 11.9 in the
199 catholyte. This produced a pH difference of 9.4 units across the PEM and increased the overpotential
200 calculated from the Nernst equation by 0.55 V, representing the largest portion of the voltage increase
201 due to NaClO_4 addition (0.67 V) (Figure 3C). Using the vapor-fed anode configuration produced a smaller
202 pH gradient across the PEM as shown by a cathode increase in pH from 5.9 to 6.9, corresponding to an
203 increase in the Nernstian overpotential of only 0.06 V (Figure 3C). The relatively small overpotential of the
204 vapor-fed anode configuration with NaClO_4 (0.16 V), indicated that the electric field limited the intrusion
205 of sodium ions in the anode chamber, and therefore the development of concentration gradients and
206 Nernst overpotential which was detrimental for the efficient operation of the cell.

207 A small portion of the increase in overpotential due to sodium in solution was related to an increase
208 in the PEM resistance.^{26–28} Sodium ions have higher affinity than protons toward the sulfonic groups of
209 the PEM, thus lower membrane diffusivity, increasing the resistance of the membrane in ion transport.^{27,28}
210 The EIS analysis with sodium perchlorate in solution revealed that the ohmic resistance of the liquid-
211 anolyte electrolyzer was 61% higher ($0.29 \Omega \text{ cm}^2$) than that obtained using deionized water ($0.18 \Omega \text{ cm}^2$)
212 (Figure 3C, Figure S3). This higher resistance with sodium in the electrolyte therefore contributed up to
213 0.11 V to the cell overpotential at 1 A cm^{-2} , or about 18% of the increased in overpotential by using NaClO_4
214 in the liquid-anolyte electrolyzer (Figure 3C). Using the vapor-fed anode configuration promoted proton
215 migration from the anode through the PEM, achieving minimal sodium ion diffusion into the membrane,
216 as shown by a smaller increase of the ohmic resistance in the vapor-fed anode configuration (44%, from
217 $0.18 \Omega \text{ cm}^2$ to $0.26 \Omega \text{ cm}^2$) compared to the liquid-anolyte configuration, corresponding to an
218 overpotential of 0.08 V, contributing to 50% of the increased overpotential (Figure 3C). In the vapor-fed
219 anode configuration, due to the absence of the electrolyte in the anode chamber, the sodium ions are
220 continuously replenished only in the cathode chamber, and their diffusion in the membrane is minimized
221 by the electric field, which favors the migration of positive ions from anode to cathode. Thus, the protons
222 generated by the OER at the anode are primarily used for maintaining charge balance across the cell, and
223 the water required by the OER is provided by the vapor stream and transport across the PEM.

224 The much larger impact of the increased Nernst overpotential than that due to a reduction in
225 membrane conductivity is analogous to that previously reported for pH shifts in anion exchange
226 membrane fuel cells (AEMFC) due to bicarbonate ion transport.²⁹ In that study it was found that the
227 bicarbonate from CO_2 can compete with the hydroxide ions for transport across the AEM, increasing the
228 cell overpotential. Adding 400 ppm of CO_2 at 1 A cm^{-2} increased the overpotential by 281 mV, with only

229 9% (25 mV) due to the decrease in membrane conductivity. The largest portion (58%, 162 mV) of the
230 increased overpotential resulted from the Nernst overpotential due to concentration gradient, with the
231 remainder caused by charge transfer losses (33%, 94 mV). The same relative decreases in overpotentials
232 resulted here using two liquid electrolytes with Na⁺ ions in solution where the greatest proportion of the
233 increased electrolyzer overpotential was due to the development of a pH gradient compared to a much
234 smaller overpotential due to the increased membrane resistance.

235

236 *Using a saltwater catholyte in the vapor-fed anode electrolyzer.*

237 We investigated the Faradaic efficiency toward the OER using sodium chloride solutions
238 representative of brackish water (NaCl 50 mM, 3 g L⁻¹) and seawater (NaCl 0.5 M, 30 g L⁻¹). When chloride
239 ions were used in the liquid catholytes there was no significant amount of chlorine generation in the
240 vapor-fed anode electrolyzer based on the measured Faradaic efficiencies. The vapor-fed anode
241 electrolyzer had a Faradaic efficiency of 100 ± 1 % for oxygen using impaired water (50 mM NaCl) in the
242 feed at current densities up to 1 A cm⁻² (Figure 3D). Even though the FE with NaCl 50 mM averaged 100%
243 for the anode, small traces of Cl₂ were generated as shown by a small amount of Cl₂ detected in the anode
244 liquid reservoir (4.5 ± 0.4 μmol h⁻¹), equivalent to 0.1% of the FE. Therefore, under these conditions there
245 was very little transport of chloride ions from the catholyte to the anode. Tests were not conducted using
246 NaCl solutions in both chambers in order to avoid damage to the system that would result from very high
247 chlorine generation rates.

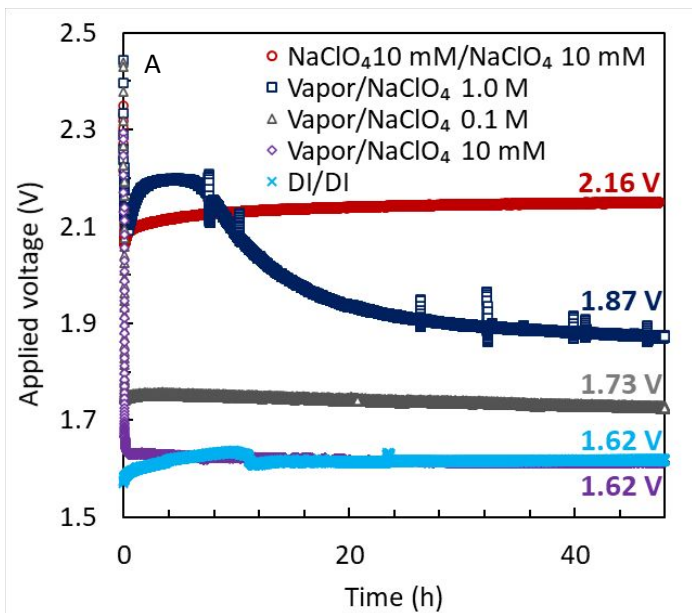
248 Even at NaCl concentrations analogous to salt concentrations in seawater (0.5 M NaCl), Faradaic
249 efficiencies remained very high (96 ± 2 %) in the vapor-fed anode electrolyzer. The much higher chloride
250 concentrations in the cathode chamber with 0.5 M NaCl resulted in more substantial Cl⁻ transport across
251 the PEM into the anode chamber that resulted in the reduced FE. Based on the decrease in the FE the
252 amount of Cl₂ produced with NaCl 0.5 M was 1.9 mmol h⁻¹, but only a small fraction (24.8 ± 0.5 μmol h⁻¹
253 corresponding to 0.5% FE) of it was detected in the anolyte reservoir likely due to volatilization or
254 oxidation of the electrolyzer components.

255 Sodium ions in the NaCl 50 mM solution increased the cell overpotential due to the development of
256 a pH gradient across the cell. In the vapor-fed anode electrolyzer fed NaCl 50 mM the cell voltage was
257 0.29 V (2.03 ± 0.01 V) larger than that obtained with a DI catholyte (1.74 ± 0.01 V), although this was 0.41
258 V lower than the cell voltage of the liquid-anolyte electrolyzer with a lower sodium concentration of 10
259 mM NaClO₄ (2.44 ± 0.00 V) (Figure 3A, 3B). Larger concentrations of NaCl (0.5 M) substantially increased
260 the cell voltage to 2.45 ± 0.02 V. Each increase in the cell overpotential was accompanied by an increase

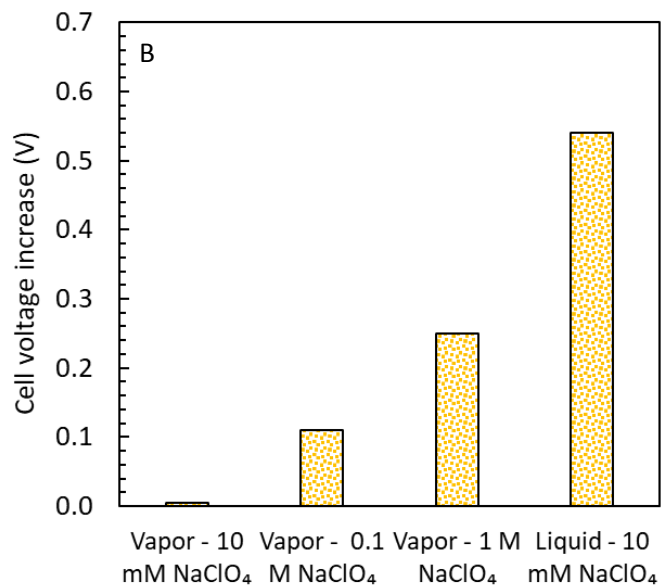
261 in the pH gradient across the PEM. The pH difference between anode and cathode was 3.4 units of pH
262 with NaCl 50 mM, corresponding to a Nernst overpotential due to that pH gradient of 0.20 V. With 0.5 M
263 NaCl, the pH difference between anode and cathode increased to 8 units of pH (anode pH of 2.9 and a
264 cathode pH of 11.3), increasing the Nernst overpotential by 0.5 V. Thus, the development of a pH gradient
265 in the vapor-fed anode configuration was affected by the sodium concentration in the cathode chamber.
266

267 *Impact of sodium ions on the vapor-fed anode electrolyzer performance with Nafion 117.*

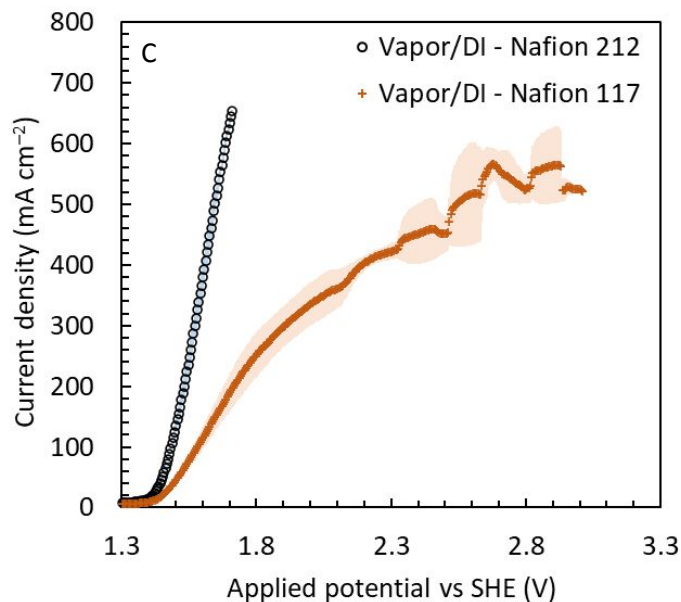
268 The impact of the presence of sodium ions in solution on electrolyzer overpotentials was investigated
269 with a thicker membrane (Nafion 117, 183 μm) using different NaClO_4 concentrations in the catholyte.
270 The cell voltage in the vapor-fed anode configuration was not affected by NaClO_4 concentrations up to 10
271 mM (1.62 V) but it increased by 0.11 V with 0.1 M NaClO_4 (1.73 V) compared to DI (1.62 V) (Figure 4A, 4B).
272 The voltage of the vapor-fed electrolyzer using 1 M NaClO_4 as a catholyte initially increased up to 2.19 V
273 and then slowly diminished until reaching 1.87 V (0.25 V additional voltage compared to DI), likely due to
274 the purging of the sodium ions which entered the membrane during startup. These cell voltages are all
275 lower than those obtained when feeding the same solutions containing NaClO_4 into the liquid anolyte.
276 The cell voltage was 0.55 V larger (2.16 V) using a 10 mM NaClO_4 solution as the anolyte and catholyte
277 compared to the same configuration with DI (1.62 V). The overpotentials due to the sodium of the vapor-
278 fed anode electrolyzer with Nafion 117 were also lower than those obtained with the thinner Nafion 212
279 in NaClO_4 solutions (Figure 3A, 3B). With the thinner Nafion 212 (50.8 μm), the cell voltage increased by
280 0.16 V with 10 mM NaClO_4 in the catholyte, compared to no change in the cell voltage using the same
281 solution with Nafion 117. The electrolyzer voltage increased by only 0.11 V in a 10 \times more concentrated
282 NaClO_4 solution (0.1 M). Thus, using thicker PEMs (Nafion 117 instead of Nafion 212) limited the
283 development of large overpotentials in the presence of high concentration of sodium ions in the vapor-
284 fed anode configuration. Therefore, the concentration gradient that developed across the cell depends
285 on the thickness of the PEM separating the electrodes.



286



287



288

289 **Figure 4.** (A) Chronoamperometries at 60 mA cm^{-2} and (B) correspondent overpotentials due to sodium
 290 with different concentration of NaClO_4 in the catholyte of the vapor-fed anode electrolyzer compared to
 291 a liquid-anolyte electrolyzer fed with DI in anode and cathode chambers separated by Nafion 117. (C)
 292 Linear sweep voltammeteries in the vapor-fed anode configuration with different membrane thicknesses.
 293 Increasing the PEM membrane thickness from $51 \mu\text{m}$ (Nafion 212) to $183 \mu\text{m}$ (Nafion 117) result in the
 294 development of a mass-transfer controlled regime at high current densities.

295

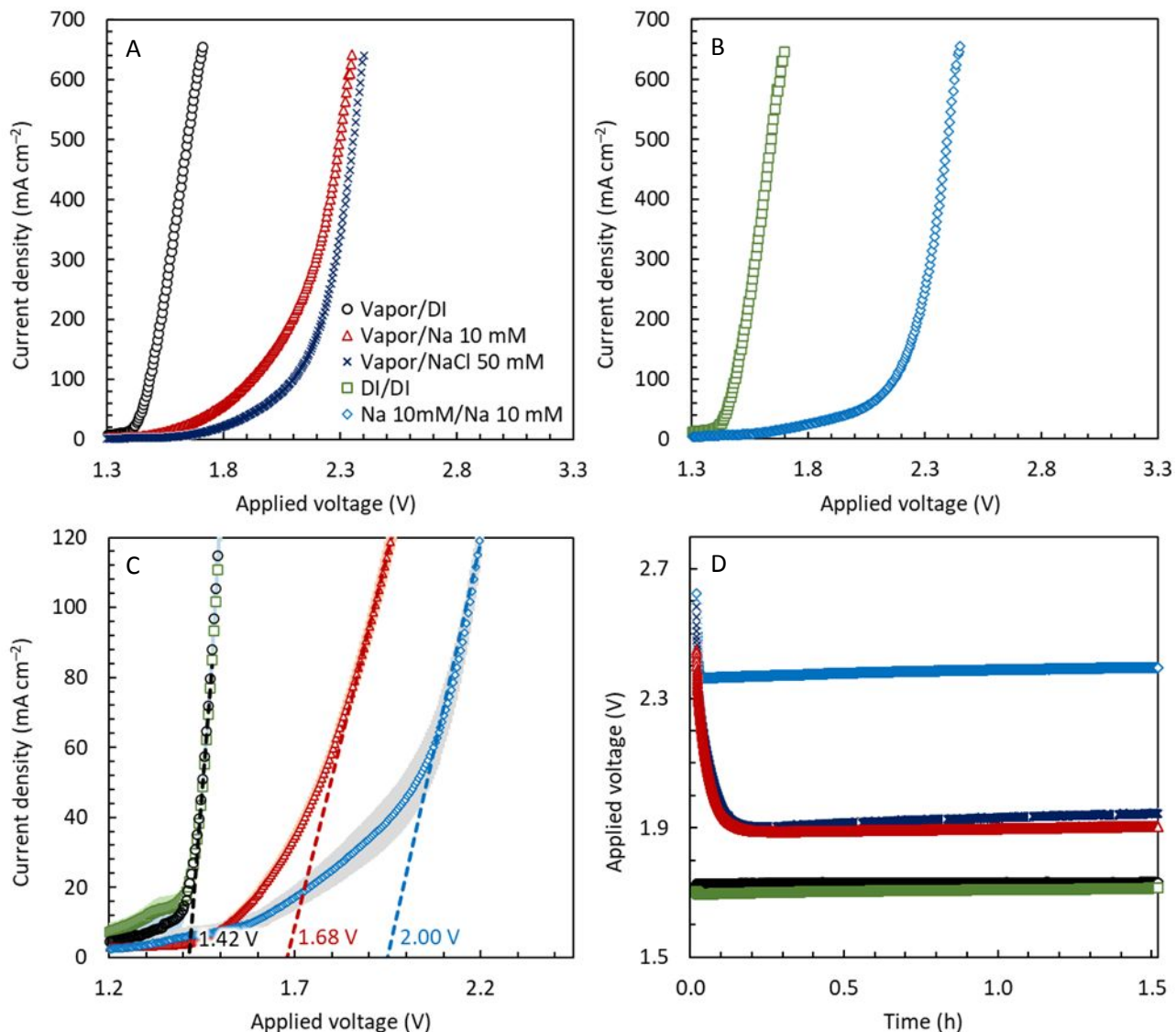
296 Using Nafion 117 limited the maximum current density that can be delivered by the vapor-fed
 297 electrolyzer, despite the reduced cell overpotentials in the presence of sodium ions. While no apparent
 298 limiting current density was reached with Nafion 212 ($50.8 \mu\text{m}$) up to 1 A cm^{-2} , a maximum current density
 299 of 0.6 A cm^{-2} was obtained using Nafion 117 ($183 \mu\text{m}$), likely due to the reduced water flux from the
 300 cathode to anode (Figure 4C). This limiting current density is slightly lower than that previously obtained
 301 (0.8 A cm^{-2}) when pure water was fed only at the cathode of an electrolyzer using Nafion 117. In that
 302 study, when Nafion 117 was replaced with Nafion 212, the limiting current density increased to 2.4 A cm^{-2} .
 303 ^{2,30} The transport of water through the PEM depends on the pressure in the cathode chamber and the
 304 thickness of the membrane.^{30,31} The OER consumes water (eq. 1), thus maintaining sufficient water at the
 305 anode through humidification and diffusion through the membrane is critical for operation of the
 306 electrolyzer (Figure S4).³⁰ In the vapor-fed anode electrolyzer, water molecules can diffuse from the
 307 cathode to the anode due to the concentration gradient, and the humidified gas stream helps to keep the
 308 anode wet and provide H_2O molecules for the OER.²² However, each proton migrating under the effect of
 309 the electric field transports 1-3 water molecules away from anode to the cathode.^{32,33} At high currents,
 310 the migration of ions coupled with water consumption by the OER will increase water losses relative to

311 that provided by the humidified air or water diffusion from the cathode, resulting in drying of the anode
312 and PEM, limiting the electrolyzer performance. Thus, a trade-off exists in the choice of the PEMs in the
313 vapor-fed anode configuration, with thinner membranes enabling higher current densities of the
314 electrolyzer but allowing higher sodium ion transport to the anode compared to thicker membranes. The
315 sodium ions in the anode chamber can migrate back in the cathode chamber under the effect of the
316 electric field, contributing to increase the cell overpotentials due to the development of pH gradients
317 across the cell.

318

319 *Electrochemical characterization of the vapor-fed anode electrolyzer.*

320 The vapor-fed anode electrolyzer showed similar performance in LSVs compared to the liquid-anolyte
321 electrolyzer when fed with ultrapure water (Figure 5A and B). The cell voltage of the liquid-anolyte
322 electrolyzer fed DI water was 1.64 V at 0.5 A cm^{-2} , similar to that obtained in the vapor-fed anode
323 configuration (1.65 V at 0.5 A cm^{-2}). Adding as low as 10 mM sodium perchlorate in the solution of a liquid-
324 anolyte electrolyzer increased the cell voltage at 0.5 A cm^{-2} of 0.8 V to 2.40 V compared to a DI/DI
325 configuration (1.64 V) (Figure 5B). The vapor-fed anode electrolyzer produced similar current densities of
326 the liquid-anolyte electrolyzer at voltages around 0.1 V smaller. For example, at 0.5 A cm^{-2} the cell voltage
327 of the vapor-fed anode electrolyzer was 2.30 V, but further increasing the concentration of sodium to 50
328 mM and 0.5 M increased the cell voltage to 2.37 V, similar to that obtained in the liquid-anolyte
329 configuration with sodium 10 mM (2.40 V) (Figure 5A). Using sodium perchlorate 10 mM as electrolyte
330 shifts the onset voltage by more than 0.6 V from 1.42 V to 2.00 V for the liquid-anolyte configuration and
331 by 0.3 V for the vapor-fed anode electrolyzer compared to the configurations using pure water (Figure
332 5C).



333
 334 **Figure 5.** LSVs of the (A) vapor-fed anode and (B) liquid-anolyte configurations containing different sodium
 335 concentrations in solution. (C) Onset potentials for the vapor-fed anode and liquid-anolyte configurations
 336 fed electrolytes with different ionic concentrations based on the linear region as shown. The current
 337 density range used for the linearization was 80 – 120 mA cm⁻². (D) Chronoamperometries at 0.5 A cm⁻²
 338 with different concentration of ions in the electrolyte fed to both anode and cathode or only at the
 339 cathode.
 340

341 The shift in the onset voltage of 0.3 V for the vapor-fed anode configuration with 10 mM sodium
 342 perchlorate as a catholyte was larger than the cell voltage shift obtained in the chronoamperometry at 1
 343 A cm⁻² (Figure 3A, 3B). Thus, we investigated the impact on the cell voltage of the application a constant
 344 current in the different electrolyzer configurations. Driving constant current through the vapor-fed anode
 345 electrolyzer reduced the cell overpotential when sodium ions were present in the catholyte over time
 346 (Figure 5D). At 0.5 A cm⁻² the cell voltage decreased from 2.45 V to 1.90 V with sodium perchlorate 10

347 mM and from 2.55 V to 1.93 V with NaCl 50 mM after only one hour of operation. Such cell voltages were
348 0.2 V larger with NaClO₄ 10 mM and NaCl 50 mM compared to that obtained with ultrapure water and
349 similar to that obtained in the chronoamperometry at 1 A cm⁻² (0.2 V with NaClO₄ 10 mM and 0.2 V with
350 NaCl 50 mM), indicating that constant currents shall be applied to completely exploit the advantages of
351 the vapor-fed anode configuration in decreasing the cell overpotentials. The decrease in the cell voltage
352 over time was likely due to the progressive removal of sodium ions from the PEM under the effect of the
353 electric field, contributing to diminish the development of large differences of pH between anode and
354 cathode. The voltages of the liquid-anolyte configuration fed ultrapure water or sodium perchlorate 10
355 mM did not change during the chronoamperometry (Figure 5D).

356

357 **Conclusions**

358 Using a vapor-fed anode configuration and a saltwater catholyte minimized chlorine generation in the
359 anode chamber, leveraging the selectivity of the PEM in rejecting the chloride ions from the cathode
360 chamber. A Faradaic efficiency of 100 ± 1% was obtained using NaCl 50 mM (3 g L⁻¹) as a catholyte, and it
361 was reduced to only 96 ± 2% with NaCl 0.5 M (30 g L⁻¹). The use of specific anode catalysts that minimize
362 the CER could further reduce the generation of chlorine in these vapor-fed anode electrolyzers. The
363 absence of a liquid anolyte limited the sodium diffusion through the PEM, as positive ions were primarily
364 migrating from anode to cathode to balance the charge, avoiding the development of large pH gradients
365 across the PEM. The cell voltage increased by only 9% (vapor-DI, 1.74 ± 0.01 V; vapor-NaClO₄ 10 mM, 1.90
366 ± 0.01 V) in a vapor-fed anode configuration, compared to a much larger increase of 40% for the
367 electrolyzer fed with a liquid anolyte containing sodium ions (DI-DI, 1.77 ± 0.01 V; NaClO₄ 10 mM- NaClO₄
368 10 mM, 2.44 ± 0.00 V), due to a lower pH gradient in the vapor-fed anode configuration (1 unit of pH)
369 compared to the liquid-anolyte configuration (9 units of pH). Using thicker PEMs (Nafion 117 - 183 μm vs
370 Nafion 212 - 50.8 μm) in the electrolyzer allowed to further diminish the overpotential due to sodium
371 contamination but lowered the maximum current density to 0.6 A cm⁻² in the vapor-fed anode
372 configuration. This new configuration can advance current PEM electrolyzer technologies towards the use
373 of impaired waters as it showed that commercial water electrolyzer with PEM can be used with a seawater
374 feed with little to no modification in the system architecture at current densities relevant for their
375 application. The stability over several months and the complete suppression of the CER with dedicated
376 anode catalysts will be next technical challenge for development of a practical system.

377

378 **Literature cited**

- 379 1 F. B. Bendixen, W. L. Eriksen, K. Aasberg-petersen, C. Frandsen, I. Chorkendorff and P. M.
380 Mortensen, *Science*, 2019, **759**, 756–759.
- 381 2 W. Tong, M. Forster, F. Dionigi, S. Dresp, R. Sadeghi Erami, P. Strasser, A. J. Cowan and P. Farràs,
382 *Nat. Energy*, 2020, **5**, 367–377.
- 383 3 J. N. Galloway, A. R. Townsend, J. W. Erisman, M. Bekunda, Z. Cai, J. R. Freney, L. A. Martinelli, S.
384 P. Seitzinger and M. A. Sutton, *Science*, 2008, **320**, 889–892.
- 385 4 Y. Kuang, M. J. Kenney, Y. Meng, W. H. Hung, Y. Liu, J. E. Huang, R. Prasanna, P. Li, Y. Li, L. Wang,
386 M. C. Lin, M. D. McGehee, X. Sun and H. Dai, *Proc. Natl. Acad. Sci. U. S. A.*, 2019, **116**, 6624–6629.
- 387 5 L. Yu, Q. Zhu, S. Song, B. McElhenny, D. Wang, C. Wu, Z. Qin, J. Bao, Y. Yu, S. Chen and Z. Ren,
388 *Nat. Commun.*, 2019, **10**, 1–10.
- 389 6 L. Shi, R. Rossi, M. Son, D. M. Hall, M. A. Hickner, C. A. Gorski and B. E. Logan, *Energy Environ. Sci.*,
390 2020, **13**, 3138–3148.
- 391 7 S. Dresp, F. Dionigi, M. Klingenhof and P. Strasser, *ACS Energy Lett.*, 2019, **4**, 933–942.
- 392 8 S. Khatun, H. Hirani and P. Roy, *J. Mater. Chem. A*, 2021, **9**, 74–86.
- 393 9 F. Dionigi, T. Reier, Z. Pawolek, M. Gliech and P. Strasser, *ChemSusChem*, 2016, **9**, 962–972.
- 394 10 S. S. Veroneau and D. G. Nocera, *Proc. Natl. Acad. Sci. U. S. A.*, 2021, **118**, 1–5.
- 395 11 S. Dresp, T. Ngo Thanh, M. Klingenhof, S. Brückner, P. Hauke and P. Strasser, *Energy Environ. Sci.*,
396 2020, **13**, 1725–1729.
- 397 12 J. N. Hausmann, R. Schlögl, P. W. Menezes and M. Driess, *Energy Environ. Sci.*, ,
398 DOI:10.1039/d0ee03659e.
- 399 13 J. G. Vos and M. T. M. Koper, *J. Electroanal. Chem.*, 2018, **819**, 260–268.
- 400 14 J. G. Vos, T. A. Wezendonk, A. W. Jeremiasse and M. T. M. Koper, *J. Am. Chem. Soc.*, 2018, **140**,
401 10270–10281.
- 402 15 L. Zhang, X. Jie, Z. G. Shao, Z. M. Zhou, G. Xiao and B. Yi, *Int. J. Hydrogen Energy*, 2012, **37**, 1321–
403 1325.
- 404 16 L. Zhang, X. Jie, Z. G. Shao, X. Wang and B. Yi, *J. Power Sources*, 2013, **241**, 341–348.
- 405 17 S. Dresp, F. Dionigi, S. Loos, J. Ferreira de Araujo, C. Spöri, M. Gliech, H. Dau and P. Strasser, *Adv.*
406 *Energy Mater.*, 2018, **8**, 1800338.
- 407 18 C. Xiang, K. M. Papadantonakis and N. S. Lewis, *Mater. Horizons*, 2016, **3**, 169–173.
- 408 19 B. L. Kienitz, H. Baskaran and T. A. Zawodzinski, *Electrochim. Acta*, 2009, **54**, 1671–1679.
- 409 20 R. A. Rozendal, T. H. J. A. Sleutels, H. V. M. Hamelers and C. J. N. Buisman, *Water Sci. Technol.*,
410 2008, **57**, 1757–1762.
- 411 21 G. M. Geise, H. J. Cassidy, D. R. Paul, B. E. Logan and M. A. Hickner, *Phys. Chem. Chem. Phys.*,
412 2014, **16**, 21673–21681.
- 413 22 J. M. Spurgeon and N. S. Lewis, *Energy Environ. Sci.*, 2011, **4**, 2993–2998.
- 414 23 S. Kumari, R. Turner White, B. Kumar and J. M. Spurgeon, *Energy Environ. Sci.*, 2016, **9**, 1725–
415 1733.
- 416 24 W. Xu and K. Scott, *Int. J. Hydrogen Energy*, 2010, **35**, 12029–12037.
- 417 25 R. A. Rozendal, H. V. M. Hamelers and C. J. N. Buisman, *Environ. Sci. Technol.*, 2006, **40**, 5206–
418 5211.
- 419 26 I. A. Stenina, P. Sistas, A. I. Rebrov, G. Pourcelly and A. B. Yaroslavtsev, *Desalination*, 2004, **170**,
420 49–57.
- 421 27 J. G. Goodwin, K. Hongsirikarn, S. Greenway and S. Creager, *J. Power Sources*, 2010, **195**, 7213–
422 7220.
- 423 28 T. Okada, H. Satou, M. Okuno and M. Yuasa, *J. Phys. Chem. B*, 2002, **106**, 1267–1273.
- 424 29 Y. Zheng, T. J. Omasta, X. Peng, L. Wang, J. R. Varcoe, B. S. Pivovar and W. E. Mustain, *Energy*
425 *Environ. Sci.*, 2019, **12**, 2806–2819.
- 426 30 M. Müller, M. Carmo, A. Glüsen, M. Hehemann, S. Saba, W. Zwaygardt and D. Stolten, *Int. J.*

- 427 *Hydrogen Energy*, 2019, **44**, 10147–10155.
428 31 Q. Duan, H. Wang and J. Benziger, *J. Memb. Sci.*, 2012, **392-393**, 88–94.
429 32 Y. K. Choe, E. Tsuchida, T. Ikeshoji, S. Yamakawa and S. A. Hyodo, *J. Phys. Chem. B*, 2008, **112**,
430 11586–11594.
431 33 T. A. Zawodzinski, C. Derouin, S. Radzinski, R. J. Sherman, V. T. Smith, T. E. Springer and S.
432 Gottesfeld, *J. Electrochem. Soc.*, 1993, **140**, 1041–1047.

433

434 **Acknowledgements**

435 The authors acknowledge funding by Penn State University.

436

437 **Competing interests**

438 The authors declare no competing interests.

439